Effect of magnetic fields on the methyl rotation in a paramagnetic cobalt(II) complex. Quasielastic neutron scattering studies

Journal:	*Physical Chemistry Chemical Physics*
Manuscript ID	CP-ART-03-2018-001660.R2
Article Type:	Paper
Date Submitted by the Author:	06-Jul-2018
Complete List of Authors:	Stavretis, Shelby; Univ Tennessee, Department of Chemistry Mamontov, Eugene; Oak Ridge National Laboratory, Spallation Neutron Source Moseley, Duncan; Univ Tennessee, Department of Chemistry Cheng, Yongqiang; Oak Ridge National Laboratory, Daemen, Luke; Oak Ridge National Laboratory, Ramirez-Cuesta, Anibal; ORNL, Neutron Science Directorate Xue, Zi-Ling; Univ Tennessee, Department of Chemistry

SCHOLARONE™
Manuscripts

Effect of magnetic fields on the methyl rotation in a paramagnetic cobalt(II) complex. Quasielastic neutron scattering studies

Shelby E. Stavretis,[1] Eugene Mamontov,[2,*] Duncan H. Moseley,[1] Yongqiang Cheng,[2] Luke L. Daemen,[2] A. J. Ramirez-Cuesta,[2] Zi-Ling Xue[1,*]

[1] *Department of Chemistry, University of Tennessee, Knoxville, Tennessee 37996, United States*

[2] *Chemical and Engineering Materials Division, Oak Ridge National Laboratory, Oak Ridge, Tennessee 37830, United States*

Abstract

Molecular dynamics is a fundamental property of metal complexes. These dynamic processes, especially for paramagnetic complexes under external magnetic fields, are in general not well understood. Quasielastic neutron scattering (QENS) in 0-4 T magnetic fields has been used to study the dynamics of $Co(acac)_2(D_2O)_2$ (**1-*d*$_4$**, acac = acetylacetonate). At 80-100 K, rotation of the methyl groups on the acac ligands is the dominant dynamical process. This rotation is slowed down by the magnetic field increase. Rotation times at 80 K are 5.6(3) x 10^{-10} s at 0 T and 2.04(10) x 10^{-9} s at 4 T. The QENS studies suggest that methyl groups in these paramagnetic Co(II) molecules do not behave as isolated units, which is consistent with results from earlier magnetic susceptibility studies indicating the presence of intermolecular interactions. DFT calculations show that unpaired electron spin density in **1** is dispersed to the atoms of both acac and H_2O ligands. Methyl torsions in **1-*d*$_4$** have also been observed at 5-100 K in inelastic neutron spectroscopy (INS). The QENS and INS results here help understand the dynamics of the compound in the solid state.

Introduction

Molecular dynamics in paramagnetic complexes, such as rotation of methyl groups, play an important role in determining magnetic properties like spin-lattice and spin-spin relaxations.[1,2] It is also well known that the unpaired electron (spin density) may be delocalized on ligand atoms,[1] leading to, e.g., hyperfine shift of the nuclei of the atoms in NMR spectroscopies.[3] In recent years, intense interests in single-molecule magnets (SMMs)[4] and molecular qubits[2,5-7] have led to extensive studies of paramagnetic metal complexes. While a recently reported Dy^{III}-based SMM displays magnetic hysteresis up to 60 K,[8] potential molecular qubits show relatively long coherence time at 80 K[7] or quantum coherence at room temperature.[6] The dynamics of the ligands or groups on the ligands is believed to play a major role in the magnetic relaxation processes, allowing the magnetic moment to re-orientate randomly and thus quenching the magnetic hysteresis.[8,9] It is also known that methyl group rotation is one of the factors affecting electron spin coherence (or spin-spin relaxation) time T_2 through electron-nuclear coupling.[2,10] Achey and coworkers have shown by their ^{13}C NMR studies that spin density in the SMM $[Mn_{12}O_{12}(^{13}CH_3COO)_{16}(H_2O)_4]\cdot 2^{13}CH_3COOH\bullet 4H_2O$ (Mn_{12}) is delocalized onto the methyl groups of the acetate ligands.[11,12]

Gómez-Coca and coworkers have recently reported that $Co(acac)_2(H_2O)_2$ (**1**), a Kramers ion, behaves as a field-induced SMM, displaying magnetic hysteresis at low temperatures.[13] At higher temperatures, **1** is considered to be a paramagnetic complex with unpaired electrons (S = 3/2) that are not localized but dispersed throughout the molecule, including the ligands.[14] In $Co^{II}(acac)_2(H_2O)_2$ (**1**), first-order spin-orbital coupling is quenched. Second-order interactions lead to zero-field splitting (ZFS) of the S = 3/2 electronic ground state.[13] We have recently studied spin-phonon couplings in **1**, $Co(acac)_2(D_2O)_2$ (**1-*d*$_4$**) and $Co(acac\text{-}d_7)_2(D_2O)_2$ (**1-*d*$_{18}$**) by

Raman and far-IR under magnetic fields. Couplings of *g* phonons with zero-field-split, excited magnetic levels [Kramers doublet (KD)] are observed as avoided crossings.[15] The current work studies the effect of magnetic fields on methyl rotation in **1-*d*$_4$**, part of our efforts to understand how molecular dynamics and magnetic properties of the complex are linked.

There have been few direct spectroscopic studies of the dynamics. Although the dynamics of paramagnetic complexes can be probed by a variety of methods, most often by AC susceptibility for magnetic relaxation, quasi-elastic neutron scattering (QENS) has been rarely used to study paramagnetic complexes.[16,17] QENS was employed to study a Tb-based SMM.[17] In this work, Kofu *et al*. determined the dynamics (i.e., magnetic relaxation) was activated around 20 K. The dynamics detected by QENS in the Tb-based SMM is a new relaxation process at the ns and ps timescale, which AC susceptibility studies are not able to reveal. The authors believe that the newly identified relaxation process may stem from either thermally activated tunneling in the higher excited states or unpaired electron spins coupled to the motion of H atoms near the magnetic ions.

QENS probes small energy transfer processes, that is, inelastic processes that appear almost elastic.[18,19] The translational or rotational motion of atoms or molecules cause broadening of the elastic peak around $E = 0$ cm^{-1}.[8,20,21] For metal complexes, QENS has been used to probe rotations of methyl and Cp groups,[19,22,23] an exchange between a hydride ligand and peripheral methyl groups,[24] and the magnetic relaxation in the Tb-based SMM.[17] QENS has also been used to characterize a precursor in spinel $GeCo_2O_4$ that, below its Neel temperature, becomes antiferromagnetically coupled ferromagnetic subunits.[25]

Internal rotations, such as methyl rotation in ethane and ethane-like molecules, have been the subjects of both theoretical and experimental studies since the early years of quantum

chemistry.[26-35] Hindered rotations and barriers to internal rotations contribute to the conformations of molecules. The nature of the rotations is of fundamental interest in part as the rotations determine some critical characters of the structures and functions of molecules.[30,31] The studies in the areas were discussed in the book by Lister, MacDonald and Owen.[30] However, the nature of barrier factors, even for ethane, is still debated, as reviewed by Goodman, Pophristic, Weinhold,[31] Gao and Mo.[33,34] Electronic origin of the barriers has been considered in terms of steric repulsions, electrostatic models and hyperconjugation, among others.[31,33,34]

We report here our QENS studies of $Co(acac)_2(D_2O)_2$ (**1-*d*$_4$**, Fig. 1). The acac ligands contain a total of four methyl groups per molecule of **1-*d*$_4$**. QENS has been used in conjugation with an applied magnetic field up to 4 T to probe field-dependent dynamics of **1-*d*$_4$** at 80-100 K, revealing the rotation of the methyl groups. In addition, inelastic neutron scattering (INS) of **1-*d*$_4$** has been investigated at the vibrational spectrometer VISION to examine the methyl torsion peaks and calculate the activation energy of methyl rotation. To our knowledge, this is the first time that field-dependent dynamics of the methyl rotation has been observed. Although **1-*d*$_4$** does not behave as an SMM at 80-100 K (the temperature range of the current work), the results here help understand the molecular dynamics and the effect of the magnetic fields on the dynamics.

Results and discussion

QENS data and calculations of methyl rotation times τ

To probe the temperature range where the measurable dynamical processes occur, the Backscattering Spectrometer (BASIS), a QENS instrument, was utilized. A fixed window scan, where the elastic (within the energy resolution of the spectrometer) intensity is recorded as a function of temperature, was performed on **1-*d*$_4$** as shown in Fig. 1 between 2 and 275 K. Based

on Fig. 1, the temperature range where the QENS signal could be probed by BASIS is between 70 and 120 K. Under 70 K, the dynamics is too slow to be detected by BASIS and the elastic intensity shows little temperature dependence aside from the thermal Debye-Waller factor due to the vibrational degrees of freedom that are always present. However, once the temperature is increased to ~70 K, there is a drop in elastic intensity signifying the presence of quasi-elastic behavior, or broadening of the scattering signal, at the expense of the intensity measured at ω = 0. The dynamics detected in this region is associated with classical stochastic methyl rotations.

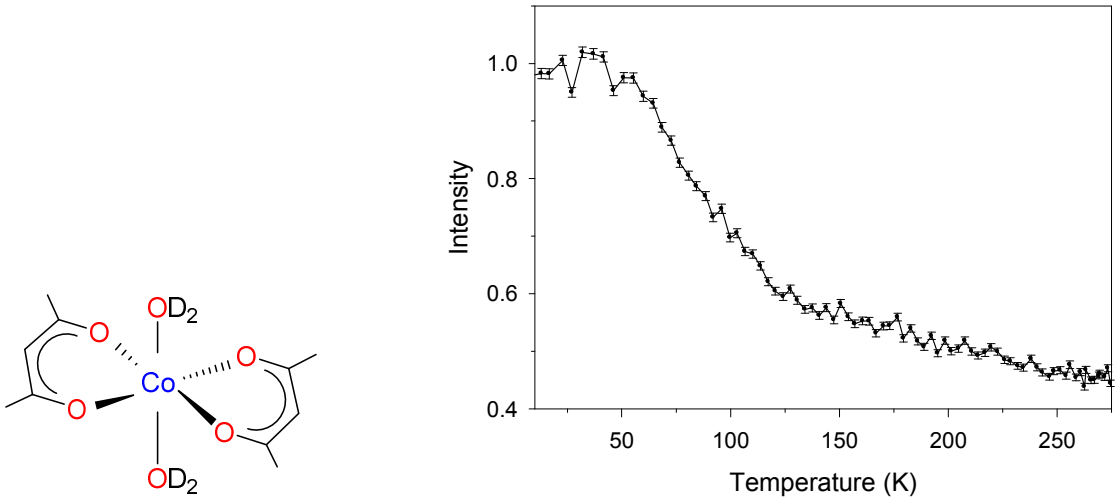

Fig. 1 (Left) Structure of **1-*d*$_4$**. (Right) Fixed window elastic scattering neutron intensity scan at $|Q|$ = 0.3 Å^{-1} between 2 and 275 K. $|Q|$ dependence of the fixed window scan is shown in Fig. S1.

QENS data at 80, 90, and 100 K show broadening compared to the resolution function of the sample measured at 2 K. Representative QENS data compared to the resolution function are given in Figs. S2-S3. The intensity of the QENS component was found to increase with Q, indicating localized motion (rather than magnetic scattering signal). The QENS data were fit with the Cole-Cole model dynamic structure factor (Eqs. 1-2). Here, the parameter E_0, indicating

the broadening of the corresponding QENS signal, is analogous to the HWHM (Γ) parameter of a Lorentzian function, which is the limiting case when the "stretching" parameter $\alpha = 0$.[36] E_0 values from these fits are shown in Tables 1 and S1. It should be noted that initially an attempt was also made to fit the data with the Lorentzian (rather than the Cole-Cole) model dynamic structure factor, but it was not successful. Thus, the data were fit using the following equations:

$$I(Q,E) = \left[x(Q)\delta(E) + \left(1 - x(Q)\right)S(Q,E)\right] \otimes R(Q,E) + B(Q,E) \quad (1)$$

where $\delta(E)$ is a delta function centered at zero energy transfer (E = 0), $x(Q)$ represents the fraction of elastic scattering in the signal, $B(Q,E)$ is a linear background term, $B(Q,E) = C_1(Q)E + C_2(Q)$, $R(Q,E)$ is the resolution function, and $S(Q,E)$ is the Cole-Cole model dynamic structure factor (Eq. 2):

$$S(Q,E) = \frac{1}{\pi E_0(Q)} \frac{(E(Q)/E_0(Q))^{-\alpha(Q)} \cos\frac{\pi\alpha(Q)}{2}}{1 + 2(E(Q)/E_0(Q))^{1-\alpha(Q)} \sin\frac{\pi\alpha(Q)}{2} + (E(Q)/E_0(Q))^{2(1-\alpha(Q))}} \quad (2)$$

The Cole-Cole scattering function is commonly used in, e.g., dielectric measurements to account for the "stretched" relaxation character in the frequency space and was more recently employed to describe QENS data.[36] A representative fit of the data is given in Fig. S3. From E_0 extracted from data fitting, it is evident that the signal becomes narrower as field increases (Table 1). For example, E_0 are 1.19(6) and 0.323(17) μeV at 0 and 4 T, respectively.

Table 1 E_0 and τ values of **1-d_4** at different temperatures and 0 and 4 T from QENS

Field	Temp (K)[a]	E_0 (μeV)[b]	τ (s)[c]
0 T	80	1.19(6)	$5.6(3) \times 10^{-10}$
	90	2.43(12)	$2.71(13) \times 10^{-10}$
	100	4.5(2)	$1.48(7) \times 10^{-10}$
4 T	80	0.323(17)[d]	$2.04(10) \times 10^{-9}$
	90	1.14(6)	$5.8(3) \times 10^{-10}$
	100	2.61(13)	$2.53(12) \times 10^{-10}$

[a] Uncertainty in temperature (σT = 0.1 K)

[b] Total uncertainties σ_{total} in E_0 are given in Table 1 here:[37] $\sigma_{total}^2 = \sigma_{ran}^2 + \sigma_{sys}^2$. Random uncertainty σ_{ran} for each E_0 value is obtained from the fitting of the QENS data using Eq. 1. Systematic uncertainty σ_{sys} in E_0 from the QENS studies here is estimated to be 5% of E_0.

[c] The largest uncertainties in τ at 0 and 4 T are 2.8×10^{-11} s and 10×10^{-10} s, respectively. These are used to calculate uncertainties in E_a and τ_0 by Eqs. S1 and S2, respectively.

[d] QENS signals as narrow as the one presented here have been measured in the past on BASIS[38-40] and backscattering spectrometers elsewhere.[41]

Methyl rotation time τ is defined to be the time needed to complete one 120° rotation[23] around the C-CH_3 bonds in the acac ligand. $1/\tau$ is thus the frequency of the methyl rotation. The τ and E_0 parameters have an inverse relationship, $\tau = \hbar/E_0$ ($\hbar = h/2\pi$; h: Planck constant). τ is also known as residence time or correlation time.[19] An increase in E_0 indicates a decrease in τ. τ values at different temperatures and 0 and 4 T fields, calculated from the E_0 values, are given in

Table 1.

Activation energies E_a of the methyl rotation at 0 and 4 T

Thermal dependence of rotation times τ vs. temperature is found to follow the Arrhenius equation (Eq. 3):

$$\tau = \tau_0 e^{E_a/k_B T} \quad (3)$$

where E_a is the activation energy or barrier of the methyl rotation, τ_0 is the pre-exponential factor and, in the current case, attempt frequency Γ_0 for 120° rotation ($\Gamma_0 = 1/\tau_0$), and k_B is Boltzmann constant.

The Arrhenius plots ln τ vs. 1000/T at 0 and 4 T are given in Fig. 2. The slopes of the fit lines give E_a for the rotation of the methyl groups in **1-*d*$_4$** at the two magnetic fields. The y-axis intercepts give τ_0. We have derived error propagation formulas (Experimental section in ESI) to estimate the uncertainties in E_a and τ_0 from such fits based on the Arrhenius equation in Eq. 3. The approach to derive the formulas is analogous to those used to derive error propagation formulas for the Eyring equation by Girolami and coworkers[42] and for the Van't Hoff equation (changes in equilibrium constant, K_{eq}, of a chemical reaction vs. temperature) by us.[43, 44]

Fittings of the Arrhenius plots in Fig. 2 give activation energies at 0 [$E_{a(H=0)}$] and 4 T [$E_{a(H=4T)}$]: $E_{a(H=0)}$ = 46(4) meV [3.7(3) x 10^2 cm^{-1}; 1.05(0.10) kcal/mol] and $E_{a(H=4T)}$ = 72(5) meV [5.8(4) x 10^2 cm^{-1}; 1.67(0.12) kcal/mol]. As expected, the rotation becomes faster (with smaller τ) when temperature is increased (Table 1). Notably, the rotation slows down at 4 T (with larger τ) and the activation energy $E_{a(H=4T)}$ for the methyl rotation in the external magnetic field is larger

than $E_{a(H=0)}$ at 0 T. In other words, methyl rotation time τ, as measured by QENS, becomes longer under the applied field.

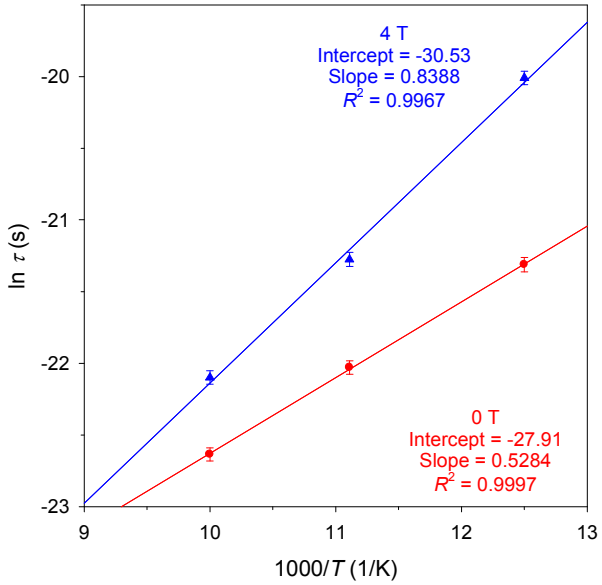

Fig. 2 Arrhenius plots of ln τ vs. 1000/T at 0 (red points and the fit line) and 4 Tesla (blue points and the fit line).

Energies of the attempt frequency Γ_0 determined are 0.86 (6.9 cm^{-1}, 0 T) and 11.8 meV (95.1 cm^{-1}, 4 T). Γ_0 from methyl rotations are typically between 2 (16 cm^{-1}) and 5 meV (40 cm^{-1}).[45] Γ_0 at 0 and 4 T are found to be field-dependent and are outside the typical range. The magnetic field effect on methyl rotations could indicate interactions between magnetic moments of the methyl groups or Co(II) ions on neighboring molecules at 0 and 4 T, which is discussed below.

The activation energy E_a may also be deduced from neutron vibrational spectroscopy. The torsions of a methyl group refer to the motions within a single potential well (or oscillations about the minimum) (Fig. 3).[30] That is, the H atoms of the CH_3 groups do *not* traverse the saddle point of the potential barrier (Fig. 3). Torsions are typically in the meV range (1 meV = 8.065

cm^{-1}) and are measurable at as low as 5 K by vibrational spectroscopies, including inelastic neutron scattering (INS). When the thermal energy in the system becomes sufficient for H atoms to overcome the potential barrier to perform a 120° jump (that is, at finite temperatures), the process is referred to as rotation or stochastic reorientation and can be measured by QENS (Fig. 3).

Peaks of methyl torsion (e.g., $\nu = 0 \rightarrow 1$ transition in Fig. 3) are observed at VISION without external magnetic field. (Currently no external magnetic field can be applied at VISION.) These peaks should be intense in the VISION spectrum since they stem from large displacements of hydrogen atoms which have a large incoherent cross section for neutron scattering.[46] At BASIS, the *effective* activation barrier is observed. No particular vibrational mode was activated in the QENS process. In other words, the temperature probed at BASIS (70-100 K) causes many modes to be activated. In comparison, using the VISION data, we are able to calculate E_a for *a particular methyl torsional mode* based on its energy. The most intense vibrational mode (methyl torsion) in the VISION spectrum is at 20.3 meV (164 cm^{-1}, Fig. 4). This mode shows strong torsions of the methyl groups. The 20.3 meV mode is used as a representative methyl torsion in the VISION data. Using the hindered methyl rotor dynamics program in DAVE[47] [methyl rotational constant = 0.65 meV (5.2 cm^{-1})], the Schrodinger equation was solved for various V_3 (height of the potential barrier). From this equation, if the ground state of 10.6 meV (85.5 cm^{-1}), V_3 is 82.0 meV (661 cm^{-1}). Then, the E_a value from the VISION data is 71.4 meV (576 cm^{-1}; 1.65 kcal/mol). Considering the two different approaches in determining E_a, the VISION data are comparable to the E_a value (~50 meV at 0 T) from the Arrhenius fitting of the BASIS data in Fig. 2. Since E_a from the BASIS data is extracted from the Arrhenius plot, the differences with the E_a extracted from the VISION data could be attributed to

either processes that are not described by the Arrhenius model, such as quantum tunneling, or the temperature dependence of the potential barrier (as QENS data are collected at 80-100 K, much higher temperatures, compared to the INS data at 5 K).[45] Analogously, the activation energy for methyl rotations in polyoligosilsesquioxanes was found to be 53.1 meV (428 cm^{-1}; 1.22 kcal/mol) and 64.7 meV (522 cm^{-1}; 1.49 kcal/mol) from the higher-temperature QENS measurement and lower-temperature INS measurement, respectively.[45]

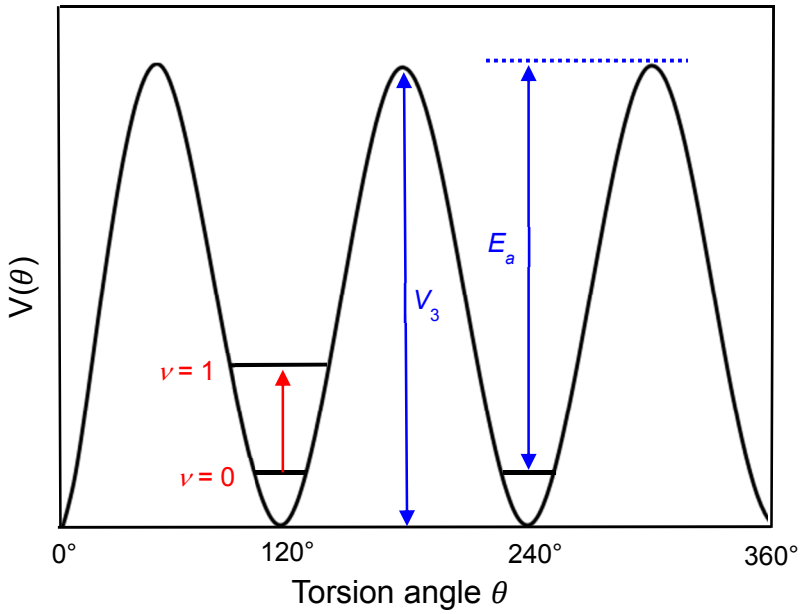

Fig. 3. Torsion and rotation of a methyl group. E_a is the activation energy of the methyl rotations; $v = 0$ is the ground torsional level; V_3 is the 3-fold barrier height.

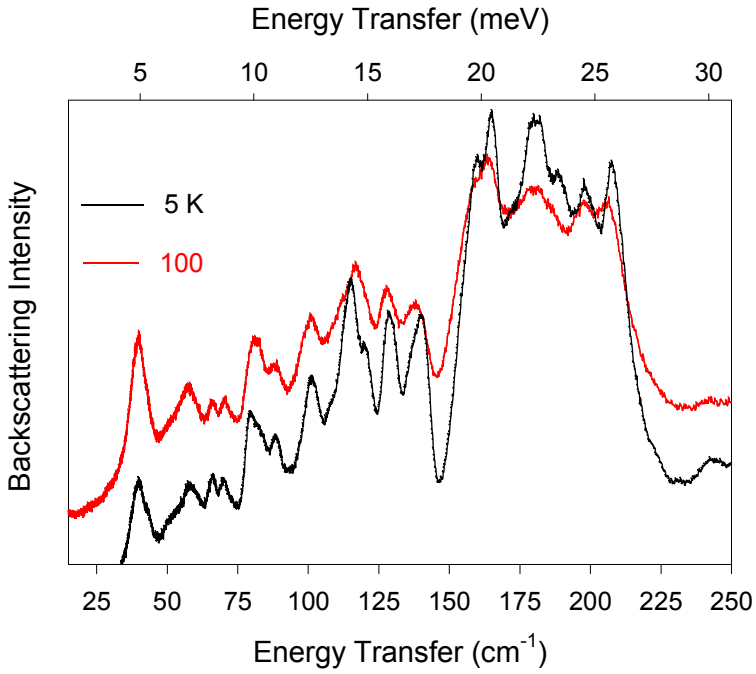

Fig. 4 INS spectra recorded at VISION (5 and 100 K) showing the strongest methyl torsion peak at 20.3 meV.

Effect of the external magnetic fields on the rotation times τ

The effect has been studied at 100 K. Rotation times from QENS were collected for a total of 10 different fields between 0 and 4 T, providing enough data points to see a trend of τ vs. the magnetic field H (Table S1). Fig. S4-Left shows an exponential trend in the rate of the methyl rotation. From 0 to 1.5 T, there is little change in τ. However, as the field is increased >1.5 T, the pace of change in τ is faster, suggesting that the observed methyl rotation is more hindered as the magnetic field is raised.

To our knowledge, how external magnetic fields affect molecular dynamics such as methyl rotation in $Co(acac)_2(D_2O)_2$ (**1-*d*$_4$**) has not been investigated. The experimental data (Table S1) show the following exponential relationship in Eq. 4:

$$\tau_{(H)} - \tau_{(H=0)} = ae^{bH} \qquad (a \text{ and } b\text{: fitting constants}) \qquad (4)$$

or the linear relationship between ln ($\tau_{(H)}$ - $\tau_{(H=0)}$) and H in Eq. 5, as demonstrated in Fig. 5:

$$\ln (\tau_{(H)} - \tau_{(H=0)}) = \ln a + bH \qquad (5)$$

If the partial electron spin on an H atom (discussed below) behaves similarly as an electron, the partial spin is expected to have two degenerate, spin-up and spin-down states. When a molecule of **1-*d*$_4$** is placed inside the external magnetic fields, Zeeman effect leads to the splitting of the spin-up and spin-down states, as is the case for an unpaired electron inside the field. Why the data in Fig. 5 give the linear relationship between ln ($\tau_{(H)}$ - $\tau_{(H=0)}$) and H in Eq. 5 deserves theoretical studies which are beyond the scope of the current work.

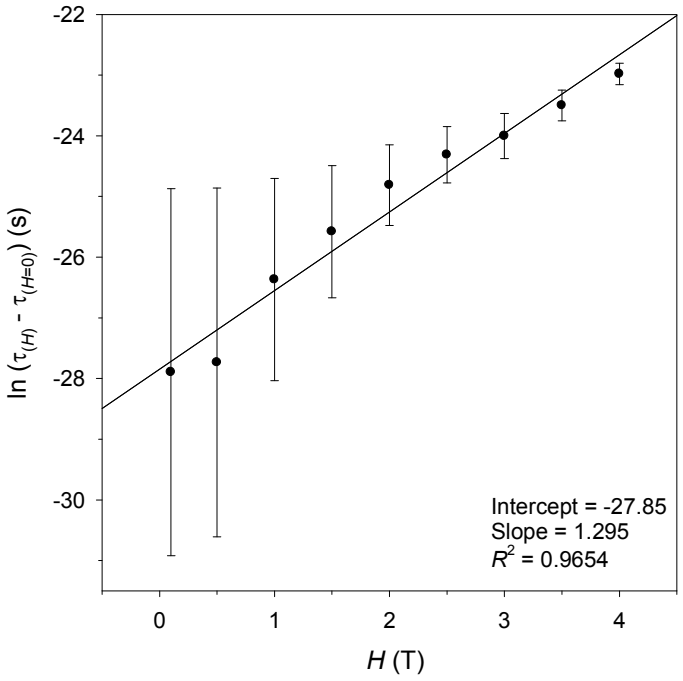

Fig. 5 Plot of ln ($\tau_{(H)}$ - $\tau_{(H=0)}$) vs H at 100 K. The larger uncertainties at smaller fields H in the

plot reflect the fact that the differences between $\tau_{(H)}$ and $\tau_{(H=0)}$ (or the numbers $\tau_{(H)}$ - $\tau_{(H=0)}$) are small. The plot $\ln(\tau_{(H)} - 0.9843\tau_{(H=0)})$ vs H gives a better fit (Fig. S4-Right) with $R^2 = 0.9932$.

Calculations of spin densities

In light of the lack of calculated spin densities for $Co(acac)_2(H_2O)_2$ (**1**), its spin densities have been calculated with the Vienna Ab Initio Simulation Package (VASP) to understand how the spin in the molecule of $Co(acac)_2(D_2O)_2$ (**1-*d*$_4$**) is dispersed onto the peripheral methyl H-atoms. It should be pointed out that the current work focuses on using QENS to probe molecular dynamics. The VASP calculations are not designed to be of high-level but were conducted to provide a quantitative scale to show the presence of spin densities on peripheral H atoms of **1**. VASP partitions electrons according to the Wigner Seitz radius a_e in Eq. 6:[48]

$$a_e = (3/4\pi n_e)^{1/3} \quad (6)$$

where n_e is electron density. Each atom is considered as a sphere and a_e defines the radius "occupied" by one atom in a sample.

This method leads to the absence of densities between atoms, i.e., densities of bonds. Therefore, the sum of the magnetic moment on all atoms combined, 2.97, is slightly smaller than the total, 3 (= 3 unpaired electrons), on the complex. The spin densities $\boldsymbol{\rho_s}$ for the atoms of **1** are given in Table 2.

The results of spin density calculations, although not at a high level, show that the unpaired electron spin density is transferred from the central Co(II) ion to the atoms of both acac and H_2O ligands. In other words, the unpaired electrons are not localized on a single point, such

as the Co(II) ion, but dispersed over the entire molecule. The results are consistent with NMR studies of such paramagnetic compounds,[3,49,50] and an earlier report by Lohr, Miller and Sharp.[51] It is well known that NMR resonances of ligands in paramagnetic complexes are typically shifted as a result of the electron spin densities on the ligand atoms.[3,49,50] Lohr and coworkers reported spin densities in $Mn(acac)_2(H_2O)_2$ ($S = 5/2$) that were calculated using the unrestricted Hartree-Fock method.[51] The spin densities on the H atoms of the methine and methyl groups have an average value of -1.5×10^{-5} and 7.2×10^{-5}, respectively. The value for the water protons is much higher at 4.3×10^{-3}. Lohr and coworkers also attempted to do the same calculations for $Co(acac)_2(H_2O)_2$ (**1**, $S = 3/2$) but indicated they could not obtain computationally significant values using their method.[51]

The transfer of spin density is probably through both spin delocalization and polarization mechanisms, as shown by the sign of $\boldsymbol{\rho_s}$ in Table 2. Such a model has been used to explain spin delocalization in paramagnetic molecules.[3,49] It should be pointed out, however, a majority of the unpaired electron spin density (~95%) is localized on the Co(II) ion. Only 0.03% unpaired electron spin is localized on the 12 H atoms of four methyl groups in the two acac ligands, while 0.3% is localized on the carbon atoms of the methyl groups. On average, each methyl group carries 7.16×10^{-5} (Table S2).

Table 2 Spin densities ρ_s of the atoms in one molecule of **1**[a]

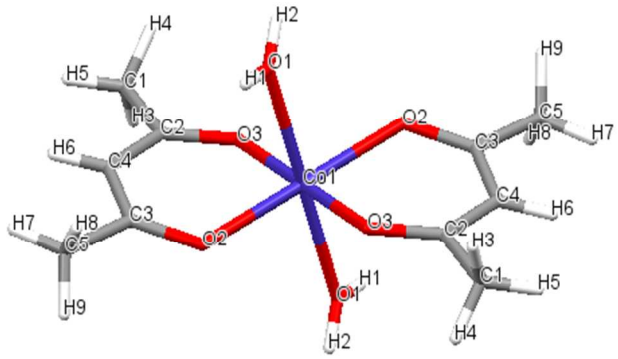

Atom	ρ_s
H6	-2.57×10^{-5}
H3-5 + H7-9	8.60×10^{-4}
H1-2	3.60×10^{-3}
C4	6.80×10^{-3}
C2-3	-3.74×10^{-3}
C1,5	8.20×10^{-3}
O2-3	1.08×10^{-1}
O1	3.81×10^{-2}
Co1	2.81
Total	2.97

[a] There are two molecules in a unit cell of **1**. The total spin density for the unit cell is twice of the total density in this table.

It is not clear why the methyl rotation is slower when magnetic field is applied. It is possible that this is due to the presence of electron spin density on the methyl hydrogen atoms. Spin density in paramagnetic complexes is known to be delocalized onto ligands,[1,3,11,12] such as the Me groups in Mn_{12}.[11,12] If the spin density on each H atom is considered as a tiny magnet, the three magnets on the three H atoms of a methyl group will align in the direction of the external magnetic field when the field is applied. In this simple, classic picture, rotating of the three magnets inside the external field is expected to be more difficult. An earlier QENS study of an exchange between the $H_{hydride}$ ligand and $H_{o\text{-methyl}}$ atoms of the mesityl group in *trans*-W(≡Cmesityl)$(dmpe)_2$H [mesityl = 2,4,6-trimethylphenyl; dmpe = 1,2-

bis(dimethylphosphino)ethane] showed that $H_{hydride}$ and $H_{o\text{-methyl}}$ atoms, which are 4.25 Å apart, undergo jump diffusion.[24] Analyses of the crystal structure of $Co(acac)_2(H_2O)_2$ (**1**) at 100 K[15] show that the H-H distances between methyl groups of neighboring molecules are as close as 2.429 and 2.547 Å. It would not be surprising that the H atoms of these methyl groups with electron spin densities have magnetic interactions among them, contributing to the intermolecular interactions between the neighboring molecules of **1**.[13] We note the calculated unpaired electron densities on the methyl H atoms are small and temperatures of 80-100 K required for this study provide large thermal energy to the H atoms.

Another possible factor is the intermolecular interactions stemming from the paramagnetic metal of the complex. Gómez-Coca *et al*. have shown that there are intermolecular interactions in the solids of $Co(acac)_2(H_2O)_2$ (**1**).[13] The interactions are significantly reduced in magnetically diluted solids of $Co_{0.05}Zn_{0.95}(acac)_2(H_2O)_2$ containing 95% diamagnetic Zn(II) ions. Such intermolecular interactions between metal centers have also been observed in other SMMs.[13,52] Inside external magnetic fields, such interactions perhaps alter the structure of two neighboring molecules, possibly making it more difficult for the methyl groups to rotate due to changes in distances between the peripheral methyl groups. However, powder neutron diffraction of $Co(acac\text{-}d_7)_2(D_2O)_2$ (**1-*d*$_{18}$**) at 0 and 7 T and 4 K using the High Resolution Powder Diffractometer (BT-1) at U.S. NIST Center for Neutron Research showed no observable structure changes beyond errors of the method.[15,53] Thus, there is no experimental data at this time to confirm such a structure change under magnetic field.

It should be pointed out that the two explanations given above are highly speculative. Additional work is needed to understand what leads to the slower rotation of the methyl groups inside magnetic fields.

Conclusions

The current work shows that external magnetic fields influence the rotations of the methyl groups in **1-*d*$_4$**. To our knowledge, this is the first report of field-dependent methyl group rotation. The variable-field QENS studies here suggest that the methyl groups on the paramagnetic molecule probably do not behave alone. The observation here is consistent with earlier magnetic susceptibility studies indicating the presence of intermolecular interactions.[13] While further work is needed to understand the origin of the changes of methyl group rotation with field, it is clear that the rotation of these groups is susceptible to magnetic field changes. Our results are different from those of Kofu *et al*.[17] as the dynamics observed here occurs at higher temperatures and is ascribed to molecular lattice dynamics instead of magnetic relaxation. The work here helps understand the dynamics in the molecules of **1-*d*$_4$** which behave as SMMs at lower temperatures.

Experimental

Complex **1-*d*$_4$** was prepared by dissolving commercial anhydrous tetramer $Co(acac)_2$ in DMF and adding D_2O to the dark purple solution, as described earlier.[15] The solution lightened and pinkish-orange crystals of **1-*d*$_4$** formed.

QENS experiments were performed at the Backscattering Spectrometer (BASIS) at the Spallation Neutron Source (SNS) at Oak Ridge National Laboratory (ORNL), Oak Ridge, TN,[54] with the following parameters. The incoming neutron wavelength band was 6.4 ± 0.5 Å. Each data point was collected for several hours. A cylindrical aluminum sample can with an inner

diameter of 12.5 mm and 5 cm of active height was used. No measurements on an empty can were taken.

In a QENS experiment, neutron scattering intensity is measured as a function of the neutron energy transfer, defined as the difference between the incident and detected neutron energy. The energy transfer range probed was ±100 μeV, whereas the Q-averaged energy resolution was 3.4 μeV, full width at half maximum. This resolution value corresponds to longest measurable relaxation time of about 0.4 ns. The Q-averaged (0.3-1.9 $Å^{-1}$) QENS spectra were fit with the Cole-Cole equation at each temperature/field. Approximately 3.8 g of polycrystalline sample of **1-*d*$_4$** was packed into a cylindrical Al sample can. This can was then topped with Al foil to prevent the powders from moving in the magnetic field. A 5 T vertical magnetic was used in the sample environment. The QENS data was fit with the Cole-Cole equation in DAVE.[47] VISION data on **1-*d*$_4$** was collected on ~2 g of samples for 1 h at 5 and 100 K. The unpaired electron spin density was calculated simultaneously with the geometry optimization of $Co(acac)_2(H_2O)_2$ (**1**) in the Vienna ab initio simulation package (VASP) with the MAGMOM tag on. Geometry optimizations were conducted on the single-crystal X-ray structure of **1** at 100 K. Spin-polarized, periodic DFT calculations were performed using VASP with the Projector Augmented Wave (PAW)[55, 56] method and the local density approximation (GGA)[57] + *U* (*U* = 5.37)[55, 58] exchange correlation functional. An energy cut off was 900 eV for the plane-wave basis of the valence electrons. Total energy tolerance for electronic structure minimization was 10^{-8} eV. The optB86b-vdW, a non-local correlation functional that approximately accounts for dispersion interactions, was applied.[59] For the structure relaxation, a 1 × 3 × 1 Monkhorst-Pack mesh was used. Wigner-seitz radius (Å): Hydrogen = 0.370; Carbon = 0.863; Oxygen = 0.820; Cobalt = 1.302. The total electron spin density is from the *s*, *p* and *d* orbitals.

The total uncertainties in the rotation time at 0 and 4 T were used in the ln τ vs 1000/T plot in Fig. 2 and error propagation calculations below. The activation energies E_a were calculated from an unweighted nonlinear least-squares procedure contained in the SigmaPlot Scientific Graph System. The uncertainties in E_a and τ_0 were computed from the following error propagation formulas (Eqs. 7 and 8), which were derived from the Arrhenius equation (Eq. 3).

$$(\sigma E_a)^2 = k_B^2 T_{max}^2 T_{min}^2 (T_{max}^2 + T_{min}^2) [\ln(\tau_{max}/\tau_{min})]^2 (\sigma T/T)^2/\Delta T^4 + 2k_B^2 T_{max}^2 T_{min}^2 (\sigma\tau/\tau)^2/\Delta T^2 \quad (7)$$

$$(\sigma\tau_0/\tau_0)^2 = 2T_{max}^2 T_{min}^2 [\ln(\tau_{max}/\tau_{min})]^2 (\sigma T/T)^2 / \Delta T^4 + (T_{max}^2 + T_{min}^2)(\sigma\tau/\tau)^2/\Delta T^2 \quad (8)$$

where $\Delta T = (T_{max} - T_{min})$.

For Arrhenius equation in the following form: $1/\tau = (1/\tau_0)\, e^{-U/kT}$ (k = Boltzmann constant), the uncertainties in U is given in Eq. 9.

$$(\sigma U)^2 = k^2 T_{max}^2 T_{min}^2 (T_{max}^2 + T_{min}^2) [\ln(\tau_{max}/\tau_{min})]^2 (\sigma T/T)^2 / \Delta T^4 + 2k^2 T_{max}^2 T_{min}^2 (\sigma\tau/\tau)^2 / \Delta T^2 \quad (9)$$

Conflicts of interest

There are no conflicts of interest to declare.

Acknowledgements

The authors thank Drs. S.O. Diallo and Craig. M. Brown for their helpful discussions and preliminary data collection. We appreciate suggestions of Profs. Xue-Tai Chen and You Song. Acknowledgement is made to the Donors of the American Chemical Society Petroleum Research Fund, National Science Foundation (CHE-1633870 to Z-L.X.) and Shull Wollan Graduate Research Fellowship (to S.E.S.) for partial support of the research. Research at the Oak Ridge National Laboratory's Spallation Neutron Source was supported by the Scientific User Facilities Division, Office of Basic Energy Sciences, U.S. Department of Energy. Computational resources for the VASP calculations were made available through the VirtuES and ICE-MAN projects, funded by the Laboratory Directed Research and Development at ORNL. We acknowledge the technical and scientific support of the staff at the SNS and the NIST for preliminary QENS data.

Notes and references

1. C. Benelli and D. Gatteschi, in *Introduction to Molecular Magnetism: From Transition Metals to Lanthanides*, Wiley-VCH, Weinheim, Germany, 2015, ch. 11, pp. 179-193.
2. M. J. Graham, J. M. Zadrozny, M. S. Fataftah and D. E. Freedman, *Chem. Mater.*, 2017, **29**, 1885-1897.
3. I. Bertini, C. Luchinat, G. Parigi and E. Ravera, *NMR of Paramagnetic Molecules: Applications to Metallobiomolecules and Models*, Elsevier, 2nd edn., 2017.
4. J. M. Frost, K. L. M. Harriman and M. Murugesu, *Chem.Sci.*, 2016, **7**, 2470-2491.
5. E. Moreno-Pineda, C. Godfrin, F. Balestro, W. Wernsdorfer and M. Ruben, *Chem. Soc. Rev.*, 2018, **47**, 501-513.
6. K. Bader, D. Dengler, S. Lenz, B. Endeward, S.-D. Jiang, P. Neugebauer and J. van Slageren, *Nat. Commun.*, 2014, **5**, 5304.

7. J. M. Zadrozny, J. Niklas, O. G. Poluektov and D. E. Freedman, *ACS Cent. Sci.*, 2015, **1**, 488-492.

8. C. A. P. Goodwin, F. Ortu, D. Reta, N. F. Chilton and D. P. Mills, *Nature*, 2017, **548**, 439-442.

9. L. Escalera-Moreno, N. Suaud, A. Gaita-Ariño and E. Coronado, *J. Phys. Chem. Lett.*, 2017, **8**, 1695-1700.

10. S. S. Eaton and G. R. Eaton, in *Distance Measurements in Biological Systems by EPR. In Biological Magnetic Resonance*, eds. L. J. Berliner, S. S. Eaton and G. R. Eaton, Klewer Academic/Plenum Publishers, 2000, vol. 19, ch. 2, pp. 29-154.

11. R. M. Achey, P. L. Kuhns, A. P. Reyes, W. G. Moulton and N. S. Dalal, *Solid State Commun.*, 2002, **121**, 107-109.

12. R. M. Achey, P. L. Kuhns, A. P. Reyes, W. G. Moulton and N. S. Dalal, *Phys. Rev. B*, 2001, **64**, 064420.

13. S. Gómez-Coca, A. Urtizberea, E. Cremades, P. J. Alonso, A. Camón, E. Ruiz and F. Luis, *Nat. Commun.*, 2014, **5**, 4300.

14. E. Ruiz, J. Cirera and S. Alvarez, *Coord. Chem. Rev.*, 2005, **249**, 2649-2660.

15. D. H. Moseley, S. E. Stavretis, K. Thirunavukkuarasu, M. Ozerov, Y. Cheng, L. L. Daemend, J. Ludwig, Z. Lu, D. Smirnov, C. M. Brown, A. Pandey, A. J. Ramirez-Cuesta, A. C. Lamb, M. Atanasov, E. Bill, F. Neese and Z.-L. Xue, *Nat. Commun.*, 2018, **9**, in press.

16. M. Appel, B. Frick, J. Elbert, M. Gallei and B. Stühn, *EPJ Web of Conf.*, 2015, **83**, 02001.

17. M. Kofu, T. Kajiwara, J. S. Gardner, G. G. Simeoni, M. Tyagi, A. Faraone, K. Nakajima,

S. Ohira-Kawamura, M. Nakano and O. Yamamuro, *Chem. Phys.*, 2013, **427**, 147-152.

18. B. Frick, in *Neutron and X-ray Spectroscopy*, eds. F. Hippert, E. Geissler, J. L. Hodeau, E. Lelièvre-Berna and J.-R. Regnard, Springer, Dordrecht, 2006, pp. 483-527.
19. M. Bée, *Quasielastic Neutron Scattering. Principles and Applications in Solid State Chemistry, Biology and Materials Science*, Adam Hilger, Bristol, U.K., 1988.
20. R. Hempelmann, *Quasielastic Neutron Scattering and Solid State Diffusion*, Oxford University Press, Oxford, 2000.
21. F. R. Trouw and D. L. Price, *Annu. Rev. Phys. Chem.*, 1999, **50**, 571-601.
22. P. Raison, G. H. Lander, A. Delapalme, J. H. Williams, R. Kahn, C. J. Carlile and B. Kanellakopulos, *Mol. Phys.*, 1994, **81**, 369-383.
23. M. Prager, H. Grimm, A. Desmedt and R. E. Lechner, *Chem. Phys.*, 2003, **292**, 161-169.
24. F. Zou, F. Furno, T. Fox, H. W. Schmalle, H. Berke, J. Eckert, Z. Chowdhury and P. Burger, *J. Am. Chem. Soc.*, 2007, **129**, 7195-7205.
25. K. Tomiyasu, M. K. Crawford, D. T. Adroja, P. Manuel, A. Tominaga, S. Hara, H. Sato, T. Watanabe, S. I. Ikeda, J. W. Lynn, K. Iwasa and K. Yamada, *Phys. Rev. B*, 2011, **84**, 054405.
26. H. H. Nielsen, *Phys. Rev.*, 1932, **40**, 445-456.
27. K. S. Pitzer, *J. Chem. Phys.*, 1937, **5**, 469-472.
28. J. D. Kemp and K. S. Pitzer, *J. Am. Chem. Soc.*, 1937, **59**, 276-279.
29. R. S. Mulliken, *J. Chem. Phys.*, 1939, **7**, 339-352.
30. D. G. Lister, J. D. MacDonald and N. L. Owen, *Internal Rotation and Inversion: Introduction to Large Amplitude Motion in Molecules*, 1978.
31. L. Goodman, V. Pophristic and F. Weinhold, *Acco. Chem. Res.*, 1999, **32**, 983-993.

32. L. H. Spangler, *Ann. Rev. Phys. Chem.*, 1997, **48**, 481-510.

33. Y. Mo and J. Gao, *Acc. Chem. Res.*, 2007, **40**, 113-119.

34. Y. Mo, *Wiley Interdiscip. Rev. Comput. Mol. Sci.*, 2011, **1**, 164-171.

35. A. E. Dorigo, D. W. Pratt and K. N. Houk, *J. Am. Chem. Soc.*, 1987, **109**, 6591-6600.

36. E. Mamontov and H. O'Neill, *Biochim. Biophys. Acta*, 2017, **1861**, 3513-3519.

37. J. R. Taylor, *An Introduction to Error Analysis: The Study of Uncertainties in Physical Measurements*, University Science Books, Mill Valley, CA, 1982.

38. D. B. Anunciado, V. P. Nyugen, G. B. Hurst, M. J. Doktycz, V. Urban, P. Langan, E. Mamontov and H. O'Neill, *J. Phys. Chem. Lett.*, 2017, **8**, 1899-1904.

39. M. Grimaldo, F. Roosen-Runge, M. Hennig, F. Zanini, F. Zhang, M. Zamponi, N. Jalarvo, F. Schreiber and T. Seydel, *J. Phys. Chem. Lett.*, 2015, **6**, 2577-2582.

40. V. K. Sharma, E. Mamontov, M. Ohl and M. Tyagi, *Phys.Chem. Chem. Phys.*, 2017, **19**, 2514-2524.

41. F. Roosen-Runge, M. Hennig, F. Zhang, R. M. J. Jacobs, M. Sztucki, H. Schober, T. Seydel and F. Schreiber, *Proc. Natl. Acad. Sci. USA,* 2011, **108**, 11815-11820.

42. P. M. Morse, M. D. Spencer, S. R. Wilson and G. S. Girolami, *Organometallics*, 1994, **13**, 1646-1655.

43. T. Chen, X.-H. Zhang, C. Wang, S. Chen, Z. Wu, L. Li, K. R. Sorasaenee, J. B. Diminnie, H. Pan, I. A. Guzei, A. L. Rheingold, Y.-D. Wu and Z.-L. Xue, *Organometallics*, 2005, **24**, 1214-1224.

44. T. Chen, Z. Wu, L. Li, K. R. Sorasaenee, J. B. Diminnie, H. Pan, I. A. Guzei, A. L. Rheingold and Z. Xue, *J. Am. Chem. Soc.*, 1998, **120**, 13519-13520.

45. N. Jalarvo, O. Gourdon, G. Ehlers, M. Tyagi, S. K. Kumar, K. D. Dobbs, R. J. Smalley,

W. E. Guise, A. Ramirez-Cuesta, C. Wildgruber and M. K. Crawford, *J. Phys. Chem. C*, 2014, **118**, 5579-5592.

46. B. S. Hudson, in *Frontiers of Molecular Spectroscopy*, ed. J. Laane, Elsevier, Amsterdam, 2009, pp. 597-622.
47. R. T. Azuah, L. R. Kneller, Y. Qiu, P. L. W. Tregenna-Piggott, C.M. Brown, J.R.D. Copley and R. M. Dimeo, *J. Res. Natl. Inst. Stan. Technol.*, 2009, **114**, 341-358.
48. P.-G. Reinhard and E. Suraud, in *Introduction to Cluster Dynamics*, Wiley-VCH Verlag GmbH, 2008, pp. 133-178.
49. G. N. La Mar, *NMR of Paramagnetic Molecules. Principles and Applications*, Academic Press, New York, 1973.
50. F. A. Walker, in *Handbook of Porphyrin Science*, eds. K. M. Kadish, K. M. Smith and R. Guilard, World Scientific, 2010, vol. 6, pp. 1-337.
51. L. L. Lohr, J. C. Miller and R. R. Sharp, *J. Chem. Phys.*, 1999, **111**, 10148-10158.
52. F. Habib, I. Korobkov and M. Murugesu, *Dalton Trans.*, 2015, **44**, 6368-6373.
53. Single-crystal (X-ray or neutron) diffraction under magnetic field is expected to offer better resolution. However, we are not aware of such a diffractometer paired with a magnet in the U.S.
54. E. Mamontov and K. W. Herwig, *Rev. Sci. Instrum.*, 2011, **82**, 085109.
55. G. Kresse and D. Joubert, *Phys. Rev. B*, 1999, **59**, 1758-1775.
56. P. E. Blöchl, *Phys. Rev. B*, 1994, **50**, 17953-17979.
57. J. P. Perdew, K. Burke and M. Ernzerhof, *Phys. Rev. Lett.*, 1996, **77**, 3865-3868.
58. F. Zhou, M. Cococcioni, C. A. Marianetti, D. Morgan and G. Ceder, *Phys. Rev. B*, 2004, **70**, 235121.

59. J. Klimeš, D. R. Bowler and A. Michaelides, *J. Phys. Condens. Matter*, 2010, **22**, 022201.